Crack Networks and Chemistry in Pyrrhotite-Affected Concrete Extracted from a Massachusetts Site

Patrick G. Dixon[(1)], Michael Mengason[(2)], David G. Goodwin, Jr.[(3)], Thomas M. Russo[(4)], Ashley S. Carey[(5)], Osamah H. Dehwah[(6, 7)], Stephanie S. Watson[(8)]

(1) National Institute of Standards and Technology, Gaithersburg, MD, USA, patrick.dixon@nist.gov

(2) National Institute of Standards and Technology, Gaithersburg, MD, USA, michael.mengason@nist.gov

(3) National Institute of Standards and Technology, Gaithersburg, MD, USA, david.goodwin@nist.gov

(4) National Institute of Standards and Technology, Gaithersburg, MD, USA, thomas.russo@nist.gov

(5) National Institute of Standards and Technology, Gaithersburg, MD, USA, ashley.carey@nist.gov

(6) PREP Associate, National Institute of Standards and Technology, Gaithersburg, MD, USA, osamah.dehwah@nist.gov

(7) Department of Civil and Systems Engineering, Johns Hopkins University, Maryland, USA, odehwah1@jh.edu

(8) National Institute of Standards and Technology, Gaithersburg, MD, USA, stephanie.watson@nist.gov

Abstract

Homes in areas of Massachusetts are experiencing issues with crumbling foundations due to pyrrhotite, similar to homes in northeastern Connecticut. Concrete from the basement of a Massachusetts home, built in the mid-1990s, experiencing pyrrhotite-driven deterioration, was cored shortly before the foundation was replaced. This paper describes analysis of three cores from one wall. The cores were subjected to resonant frequency testing, revealing dynamic Young's moduli ranging from 20.0 GPa to 4.5 GPa. These cores were then impregnated with fluorescent epoxy, sliced longitudinally, and photographed. Cracks and damage were visible in all core slices. A yellow/green selection was performed on the photographs to segment the damage. To capture the full range of plausible damage areas, a wide range of brightness thresholds was used to construct a simple damage area fraction metric. In the three cores, this metric ranges from 3.5 % to 14.3 % and decreases with increasing dynamic Young's modulus. One core was preliminarily analyzed to estimate the changes in damage over the wall thickness and imaged with micro x-ray fluorescence (µXRF). µXRF on a core section revealed sulfur-rich aggregates and a localized sulfur-rich region of cement paste, suggestive of internal sulfate attack. Further imaging of cores with µXRF and data analysis will be performed to estimate the detailed chemistry of sulfur-rich regions and understand the relationship between element distribution patterns and the observed cracks and damage.

Keywords: *cracking, dynamic elastic properties, field study, micro x-ray fluorescence, pyrrhotite*

1. INTRODUCTION

Pyrrhotite-driven deterioration of concrete foundations in afflicted areas has been associated with visible cracking patterns on the basement wall surfaces [1–5]. In Connecticut, these patterns are used in assigning a severity class to help with foundation replacement prioritization [4, 6]. These surface cracks are critical for forensic purposes, but understanding the crack network of pyrrhotite-affected concrete more holistically would provide a more complete assessment of the concrete. Indeed, several important studies have investigated cracks within the pyrrhotite-affected concrete. Jana found cracks extended through entire thickness of wall in the examinations of cores [1, 2]. Microcracking has been observed in the matrix of affected concrete in proximity to sulfate mineral deposits [3]. Additionally, microcracking has been observed within pyrrhotite-bearing aggregates [7], which pointed towards a deterioration process, accelerated by more extensive sulfate transport into the matrix through these aggregate microcracks. Titon et al. [8] have demonstrated that biotite's interlayer spaces function like roughly nanometer-sized microcracks when in proximity to pyrrhotite, enhancing the transport of the formed sulfate out of the aggregate into the cement paste.

This abstract presents a preliminary study of field samples to examine the mesoscale crack networks within a wall of a pyrrhotite-affected home in Massachusetts and the chemistry across the wall's thickness. Understanding these mesoscale crack networks will aid in assessing the structural response of pyrrhotite-affected concrete. Elemental analyses over the thickness of pyrrhotite-affected wall will provide spatial location information on the reactions. When this data is combined with the mesoscale crack network information, understanding of the relationships between the reactions and structural deterioration can be gained for the potential benefit of mitigation or even rehabilitation measures.

2. FIELDWORK

The basement of a two-story home in Massachusetts (built in the mid-1990s), experiencing deterioration consistent with pyrrhotite-driven expansion was sampled. The site featured substantial cracking in many areas along the walls. These cracks were inventoried with measurement by tape measure and crack width gauge, photographs and quick field sketches. One notable crack was a horizontal crack tapering from approximately 10 mm to 1 mm in width over a length of 3 m along one wall. This crack also intersected with a similar vertical crack running over near the full height of the wall (2 m). The slab and the wall underneath the garage showed minimal deterioration. Efflorescence was also found in areas on the walls and was sampled at multiple locations. Over 35 cores were extracted from the basement by wet coring at various locations, which were measured with tape measure, vertically from the slab and horizontally from wall corners. Locations of the wall cores were spread throughout the entirety of the basement (on 10 walls, including bump out walls in the foundation), predominantly high (approximately 1.7 m) and middle (approximately 1.1 m) positions on wall from the slab; locations were also simultaneously chosen to encompass a range of visually observed interior cracking. Cores were taken from locations, intersecting larger cracks, adjacent to larger cracks, and featuring no large observed cracks in the area, with these damage features captured in the metadata for each specimen. Six 108 mm diameter cores were removed from one wall at different positions, reflective of the described sampling. These six cores were all below the soil grade line of the wall. One core fractured during drilling or extraction from the barrel. Preliminary x-ray diffraction of the efflorescence on this wall showed thenardite as the predominant phase.

3. CORE ANALYSIS METHODS

The dynamic Young's moduli of the five intact cores of the one wall were measured with impact-driven resonant frequency testing (RFT). These tests were performed on the cores with their as-cored geometry. Namely, variable core length based on the wall thickness was possible, and both the exterior asphalt barrier and interior face of the wall were included in the samples. RFT was performed in triplicate, each measure including separate dimensional and mass measures, in addition to strikes and vibration acquisitions.

Three of the five cores, referred to as 705-F1, 707-F1, and 709-F1, at similar height along the wall and different levels of observed cracking on the interior wall surface, were then selected for sectioning. 705-F1 was closest to a wall corner, while 707-F1 was furthest. These cores were dried at 40°C for 40 hours. Each entire core was then impregnated with ultraviolet (UV)-fluorescent epoxy. The impregnated and encased cores were cut nominally in half perpendicular to their length, resulting in two cylinders per core, one with the exterior wall surface and the other with the interior wall surface. The cylinders were then sliced longitudinally twice for a middle section of nominal thickness of 6 mm using a precision saw. Orientation of the two cylinders of one core was consistently maintained during slicing, so that exterior and interior slices are the same section of the core. Water was used in all cutting operations.

All individual sections were then photographed under UV light with a Google Pixel 7a. Images of both faces of the slices were taken with and without overhead laboratory lighting to provide different contrast levels. For each section, one image was taken with a ruler without UV light for a scale reference.

Image analysis was performed in FIJI (ImageJ) [9]. The photographs were cropped to ensure that the surrounding epoxy was not included in the analysis of the core; the area analyzed for each section ranged from approximately 101 mm to 106 mm by 122 mm to 128 mm. The segmentation of the damage in the photographs with overhead laboratory lights on was performed with Hue-Saturation-Brightness

(HSB) thresholding. The full saturation range (0 to 255) was passed; the hue from 50 to 120 (0 to 255 scale) was passed, and four different thresholds were used in brightness space. The upper bound was always 255. The lower bounds for thresholding the brightness were selected based on the brightness distribution of each individual image. They were zero, the mean of the distribution minus one standard deviation of the distribution, the mean of the distribution, and the mode of the distribution. To get an initial estimate of the variation of the damage area fraction, (A_d/A_0) over the wall's thickness, approximately 20 mm (506 pixels) strips were taken from the cropped images of one face of core 709-F1, over their length, starting near the exterior and interior edges and moving towards the center of the wall. Sections less than 20 mm at the middle of the core slice were not considered.

The sections from the same core, 709-F1, were also analyzed with micro x-ray fluorescence (µXRF) with a Bruker M4 Tornado^{PLUS}. The slices were imaged under vacuum with a rhodium x-ray tube at 50 kV and 600 µA, and an x-ray spot size of 20 µm. Large area maps with step sizes of 100 µm and 35 millisecond dwell time were collected on both slices. A variety smaller-scale local maps at various locations of the wall thickness were also performed.

4. RESULTS AND DISCUSSION

The dynamic Young's moduli of the five cores spanned a large range from 20.0 GPa to 4.5 GPa. The largest absolute spread in the triplicate measures of one core was given by a standard deviation of 1.3 GPa. The largest absolute difference in the dynamic Young's moduli as measured in longitudinal and transverse modes was less than 2.0 GPa. The photographs of cores under the UV light with the overhead laboratory lights on are shown in Figure 4.1.

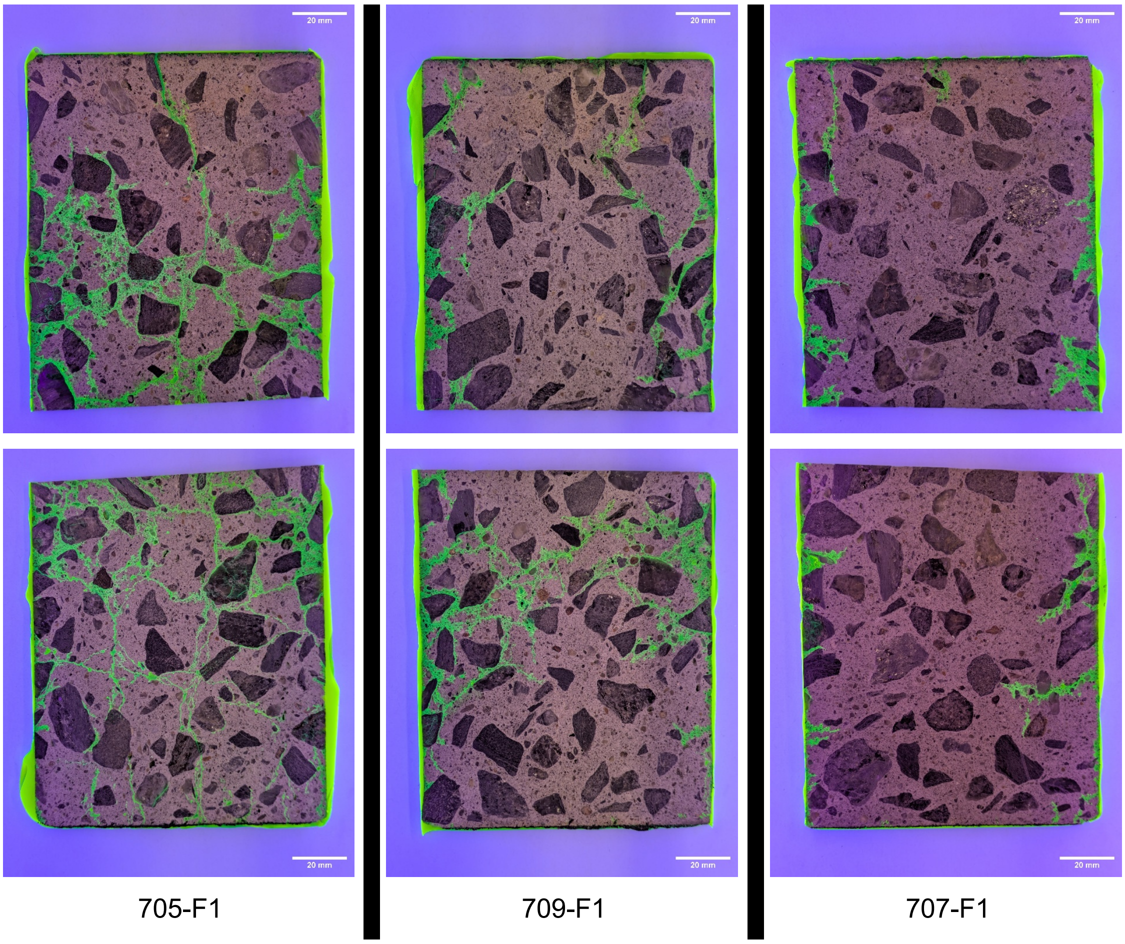

Figure 4.1: Photographs of the core sections of 705-F1, 709-F1, and 707-F1 from left to right under UV light. Interior slices are above with the interior wall edge at the top, and exterior slices are below with the exterior wall edge at the bottom. The field of view for every image above is 129 mm x 158 mm

Before discussing results, this damage should be clarified. In the procedure, the epoxy only infiltrated areas that are accessible from (i.e., connected to) the core surfaces. Smaller cracks or regions of extreme permeability that do not intersect with any of the three core surfaces are not filled with the fluorescent epoxy. Thus, the damage area fraction should be considered an estimated measure of mesoscale damage, or damage with characteristic dimensions ranging in order from hundreds of micrometers to millimeter scales. While many microcracks may be excluded in this analysis, mesoscale cracks do not constitute the only feature highlighted by the epoxy. In addition to cracks, damage regions of extreme permeability and pre-existing voids that have connectivity with the core surfaces will be highlighted by the epoxy. The HSB-based damage segmentation used in the image analysis, captures all these features. Additional work could be performed to segment various features separately, but this methodology provides a simple and consistent metric. The thresholding limits of the various damage segmentation methods were purposefully broad to ensure the inclusion of plausible damage area. The brightness threshold from zero and higher gave the highest area damage fractions, while the thresholding the brightness from the mode and higher gave the lowest. In subsequent discussion about the damage area fraction, the average of the four methods is presented followed by the minimum and maximum in parentheses, unless otherwise stated.

In Figure 4.1, it is clear there is damage in all core sections, and cracks appear over the entire thickness as found by Jana [1, 2]. Cores 705-F1 and 709-F1 exhibit considerably more damage than 707-F1, which is furthest from a wall corner and has the lowest damage area fraction, 3.5 % (2.7 %, 4.0 %). 705-F1 is the closest to a wall corner and has the largest damage area fraction, 14.3 % (10.5 %, 16.7 %). The sections of 709-F1 are the only pair of the three that shows a larger than 1 % difference of the average between the interior and exterior slice, with the exterior slice damage area fraction nearly double that of the interior. In general, damage area fractions of the two faces of the same section are quite comparable, with maximum absolute differences near 1 % for all measures. In 709-F1, the analysis over the wall thickness (length of the core) on the interior section gives damage area fractions that are not drastically spatially separated. The minimum damage area fraction of the 20 mm length subsections is 4.2 % (2.8 %, 5.0 %) centered at roughly 30 mm from the wall interior, while the maximum of 9.8 % (6.9 %, 11.7 %) is centered roughly at 50 mm from the wall interior. The analysis of the exterior section on the other hand, shows considerable differences. The subsections over the 60 mm closer to the wall exterior all show substantially lower damage area fractions. The minimum damage area fraction of 1.1 % (0.6 %, 1.4 %) is centered at roughly 10 mm from the exterior edge, while the maximum of 24.8 % (17.6 %, 29.1 %) is centered at 90 mm from the exterior edge. Qualitatively, the photographs of the other two cores also suggest more damage over the middle. The lower damage, in the vicinity of the wall interior edge, may be a result of carbonation in this area.

Figure 4.2 plots the longitudinal mode dynamic Young's modulus, E_{dyn}, against the damage area fraction, (A_d/A_0). The vertical error bars are the standard deviation of the three RFT measurements, while the horizontal bars show the minimum (mode as the lower brightness threshold) and maximum (zero as the lower brightness threshold). The trend is as expected, with the dynamic Young's modulus decreasing as the damage area fraction increases. Additionally, in Figure 4.2 the thresholding methods differ more greatly as the damage area fraction increases.

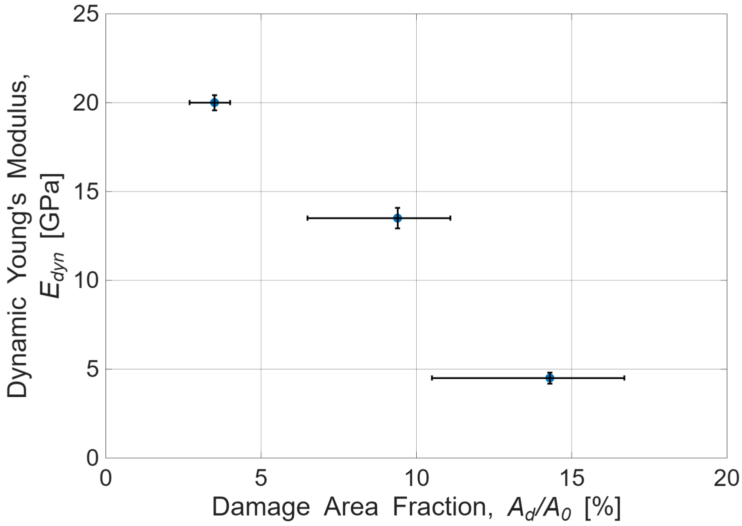

Figure 4.2: The dynamic Young's modulus (longitudinal mode) against the damage area fraction. Vertical error bars are plus/minus the standard deviation of the three, while horizontal error bars show the minimum and maximum of the damage area fraction from the four methods.

Figure 4.3 shows maps from µXRF on a subsection at middle width (middle of the core diameter) of the exterior slice of 709-F1. Figure 4.3(a) depicts the region; Figure 4.3(b) shows a µXRF chemical map and Figure 4.3(c) presents a heat map of the sulfur concentration.

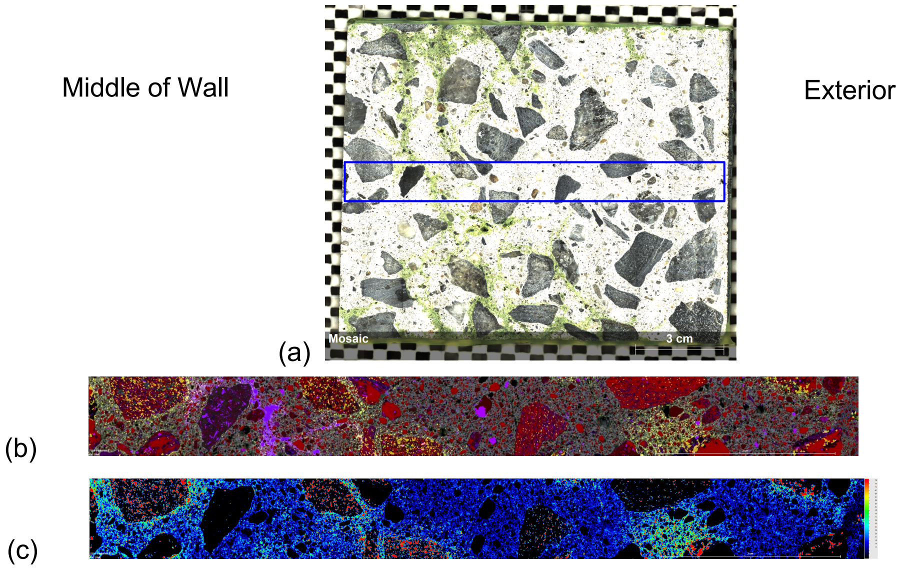

Figure 4.3: (a) The imaged subsection of the 709-F1 exterior slice; the middle of the wall is on the left and the exterior wall edge is on the right; this is consistent in subsequent images (field of view: 139 mm x 120 mm). (b) A µXRF chemical map of the subsection (Ca – green, Si – brown, S – yellow, Cl – purple; field of view: 128 mm x 13 mm). (c) The heat map of sulfur concentration from the µXRF; red is high and black is low (field of view: 128 mm x 13 mm)

Sulfur is present in both the cement paste and aggregate. Some aggregates show a very strong sulfur presence. Under first inspection, sulfur does not appear to be highly associated with the large crack, which can be located as the large purple (chlorine in the epoxy) band toward the middle (left) in Figure 4.3(b). Towards the exterior edge of the wall, there is a region of cement paste that appears to be rich in sulfate minerals. There are unlikely possibilities that this result stems from a region of cement featuring small sulfide particles or a large sulfur-bearing aggregate just below the paste, and further analysis is needed to rule these out.

5. CONCLUSIONS AND FUTURE WORK

In the three cores studied, cracks and damage are present in all and occur over their length, namely over the entire thickness of the wall. The damage area fraction ranges from 3.5 % to 14.3 % in the three cores, considering the average of four simple damage selection methods. In 709-F1, the damage area fraction tended to be greatest near the center of the wall thickness, i.e., near the middle over the core length. Further work will analyze more cores and evaluate the influence of subsection size. The dynamic Young's moduli of cores vary from 20.0 GPa to 4.5 GPa, and this property decreases with increasing damage area fraction as expected. Further work is being performed to develop the relationship between the dynamic Young's modulus and damage area fraction with the analysis of more cores. Related work is linking this nondestructive property to the conventional mechanical properties of pyrrhotite-affected concrete. µXRF is a powerful technique that permits large area examinations of the chemistry while preserving the microstructure. Sulfur is found throughout both the aggregates and cement paste. Deeper elemental analyses of the µXRF data are required to estimate the detailed chemistry.

6. DISCLAIMER

Certain equipment, instruments, software, or materials, commercial or non-commercial, are identified in this paper in order to specify the experimental procedure adequately. Such identification does not imply recommendation or endorsement of any product or service by National Institute of Standards and Technology, nor does it imply that the materials or equipment identified are necessarily the best available for the purpose.

7. ACKNOWLEDGEMENTS

Thanks to the homeowner and the contractor, Foundation Solutions of NE, LLC, for allowing NIST access to the site. Thanks also to the Federal Highway Administration for core slicing support.

References

[1] Jana D (2020) Pyrrhotite Epidemic in Eastern Connecticut: Diagnosis and Prevention. ACI Mater J 117:. https://doi.org/10.14359/51718059

[2] Jana D (2022) Cracking of residential concrete foundations in eastern Connecticut, USA from oxidation of pyrrhotite. Case Stud Constr Mater 16:e00909. https://doi.org/10.1016/j.cscm.2022.e00909

[3] Zhong R, Wille K (2018) Deterioration of residential concrete foundations: The role of pyrrhotite-bearing aggregate. Cem Concr Compos 94:53–61. https://doi.org/10.1016/j.cemconcomp.2018.08.012

[4] Connecticut Foundation Solutions Indemnity Company, Inc. (CFSIC) (2025) Connecticut Foundation Solutions Indemnity Company, Inc. ("CFSIC") Underwriting and Claims Management Program. CFSIC. https://crumblingfoundations.org/getting-started/underwriting-criteria/#prioritization. Accessed 1 December 2025

[5] Duchesne J, Fournier B, Francoeur J (2018) Study of the Deterioration of Concrete Incorporating Sulfide-Bearing Aggregates. In: ICDCS 2018. RILEM, University of Leeds, Leeds, West Yorkshire, LS2 9JT, United Kingdom, pp 273–280

[6] Santos L, Chrysochoou M, Wille K (2025) Development of a risk assessment framework for pyrrhotite induced deterioration of concrete foundations in CT and MA. Cem Concr Res 197:107951. https://doi.org/10.1016/j.cemconres.2025.107951

[7] Zhong R, Ai X, Yao Y, et al (2024) Effects of the expansion mechanisms on the pyrrhotite-induced deterioration of concrete foundations. Case Stud Constr Mater 20:e02830. https://doi.org/10.1016/j.cscm.2023.e02830

[8] Titon B, Duchesne J, Fournier B (2024) The role of biotite in the deterioration of pyrrhotite within concrete aggregates: Trois-Rivières case study. Cem Concr Res 183:107595. https://doi.org/10.1016/j.cemconres.2024.107595

[9] Schindelin J, Arganda-Carreras I, Frise E, et al (2012) Fiji: an open-source platform for biological-image analysis. Nat Methods 9:676–682. https://doi.org/10.1038/nmeth.2019